ELSEVIER

Physica B 221 (1996) 500–506

PHYSICA B

Neutron reflectivity measurements of titanium–beryllium multilayers

Alan E. Munter[a], Brent J. Heuser[a,*], Kenneth M. Skulina[b]

[a]*Department of Nuclear Engineering, University of Illinois, 214 NEL, 103 S. Goodwin Ave., Urbana, IL 61801-2984, USA*
[b]*Mechanicl Engineering Department, Lawrence Livermore National Laboratory, Livermore, CA 94551-9900, USA*

Abstract

Some of the best neutron supermirrors currently in production are made of alternating layers of nickel and titanium, with carbon added to the Ni to eliminate preferential growth. Reflectivities of 75–95% in the θ_c–$2\theta_c$ range are currently obtained from the Ni/C–Ti system. The Ti–Be multilayer system is presented here as a possible alternative to the Ni/C–Ti system. Titanium is one of the few elements which has a negative neutron scattering length, while beryllium has a relatively large positive scattering length. This makes for bilayer structures which have excellent neutron contrast, a necessary requirement of supermirror devices.

Single-bilayer-spacing Ti–Be multilayers were prepared by magnetron sputtering onto 2 mm thick silicon (0 0 1) substrates. Depositions were made with 10–80 bilayers at two different bilayer thicknesses of approximately 90 and 110 Å. Bulk layers of Ti and Be were also prepared to determine the scattering length density of each deposition component. The samples were measured at the Intense Pulsed Neutron Source (IPNS) at Argonne National Laboratory on the POSYII reflectometer. First order Bragg peak reflectivities of up to 64% were observed. Data from the two bulk depositions and one multilayer deposition have been fitted using a genetic algorithm developed at IPNS. For the bulk depositions, the scattering length densities of Ti and Be depositions are -2.2×10^{-6} and 10.3×10^{-6} Å^{-2}, respectively. In addition, results clearly indicate the presence of a 50 Å thick oxide layer on the bulk Ti deposition. The neutron scattering length density profile obtained from the neutron reflectivity measurements are in good agreement with XPS analysis of the oxide film which showed a mixture of TiO_2 and Ti_2O_3.

1. Introduction

Successful use of instrumentation found in neutron guide halls depends on the efficient transportation of long wavelength neutrons over tens of meters. This transportation, which in essence moves the neutron source much closer to the instrument, is accomplished by coating the internal surfaces of the guide conduits with a highly neutron reflective thin film. For the most effective transportation, the reflectivity and angular acceptance of the guide coatings must be maximized. The standard thin film coating material has been natural nickel (Ni) or isotopically-purified Ni-58. The angular acceptance of a neutron guide is determined by the critical angle of total reflection $(\theta_c)_b$ with natural Ni following the general rule of 0.1° per 1 Å of neutron wavelength.

The effective source area transported by a guide increases as the square of the guide acceptance angle. Accordingly, significant neutron intensity gains can be generated by extending the angular range of total reflection. Such an extension can be created by depositing a single-spacing multilayer structure in addition to a de-

*Corresponding author.

SSDI 0921-4526(95)00971-X

Table 1
Summary of Ti–Be multilayer depositions and corresponding neutron reflectivity results

Deposition	n	Peak k_z (Å^{-1})	$\Delta k_z/k_z$	Peak reflectivity	Bilayer spacing (Å)
M86	20	0.035	0.126	0.37	90
M85	40	0.036	0.108	0.48	87
M87	60	0.036	0.103	0.43	87
M88	80	0.039	0.100	0.44	81
M90	10	0.029	0.131	0.38	108
M89	20	0.028	0.107	0.60	114[a]
M91	30	0.029	0.110	0.55	108
M92	40	0.029	0.114	0.64	108
M93	Bulk Be	—	—	—	959[a]
M94	Bulk Ti	—	—	—	560[a]

[a]These values were obtained from the neutron reflectivity fitting procedure. All other multilayer spacing thicknesses were calculated from the Bragg peak position.

position of natural Ni or Ni-58. By choosing the bilayer spacing correctly, the superlattice will Bragg diffract neutrons at an angle slightly beyond the critical angle of the base coating. If several such discrete bilayer structures, each with a slightly off-set spacing, are deposited, the resulting angular acceptance can be increased well beyond θ_c [1].

The two most important criteria of a supermirror coating are (1) a large scattering length contrast between the two deposition components and (2) maintaining a flat, smooth, and uniform bilayer structure over large depositon areas. The first criteria led to the extensive testing of the nickel–titanium (Ni–Ti) system [2]. However, this system never produced the necessary reflectivities (greater than 95%) beyond θ_c of natural Ni required for neutron guide applications. In the work of Keem et al. [3], a telling problem, as demonstrated by the cross-sectional TEM, was the propagation of a defect structure up through the bilayer deposition. The end result was a distortion of the bilayer flatness over length scales greater than approximately 20 Å. Keem et al. also found that the Ni and Ti layers in their supermirror depositions were crystalline with measurable texture [3]. This suggested that a preferred growth phenomena was responsible for the bilayer distortion.

Shortly after the work of Keem et al., the addition of carbon (C) to Ni was found to improve the neutron reflectivity characteristics of Ni–Ti supermirror depositions [4, 5]. Evidently, the presence of C in the interfacial regions limits the preferred growth through the multilayer structure [6]. In fact, reflectivities of 95% out of $3\theta_c$ of natural Ni have been reported for Ni/C–Ti supermirrors [7]. However, it is not clear that this performance is reproducible; supermirror depositions investigated by Ballot et al. resulted in reflectivities of approximately 80% at $2\theta_c$ of natural Ni [8]. Although the current status of neutron supermirrors and monochromators based on the Ni/C–Ti system appears to be satisfactory, it is, in our opinion, useful to investigate other thin-film systems. It is in this context that we present prelminary neutron reflectivity studies of titanium–beryllium (Ti–Be) single bilayer-spacing multilayer depositions.

2. Experimental

A quick demonstration that Be is a worthy substitute for Ni is given by a comparison of the theoretical scattering length densities; 9.63×10^{-6} Å^{-2} and 8.83×10^{-6} Å^{-2} for Be and Ni, respectively. This very favorable comparison of Be to Ni was the primary motivation for the fabrication and subsequent characterization with neutron reflectometry of the Ti–Be multilayers presented here.

Single spacing Ti–Be multilayers, as well as bulk layers of Ti and Be, were deposited by magnetron sputtering on 2 mm thick (0 0 1) single crystal Si substrates [9]. The sputtering depositions were performed under 2.5×10^{-3} torr of argon with a source-to-substrate distance of approximately 10 cm. Deposition areas were maintained at 6 cm diameter on the 3 in. diameter substrates using a mask. All Ti–Be depositions started with the first Ti layer and ended with the last Be layer. The ten depositions fabricated using this procedure are listed in Table 1.

All data were acquired at the Intense Pulsed Neutron Source at Argonne National Laboratory using the POSY II reflectometer [10]. The POSY II reflectometer utilizes a white beam of neutrons with wavelengths ranging from 2 to 16 Å emitted by a cold moderator consisting of solid

methane at 20 K. The scattered intensities are recorded as a function of time-of-flight by a one-dimensional position sensitive detector, which measures both specular and off-specular neutrons within the incidence plane. The geometric angular resolution, $\Delta\theta$ is approximately 0.02°. The detector accepts neutrons scattered out of the reflection plane by angles up to 0.8°, and all neutrons in this range are summed and treated as reflected neutrons within the reflection plane. The data sets were collected for each sample at several angles and merged together to get a full k_z range up to approximately 0.06 Å^{-1}.

A summary of the neutron reflectivity measurements, including the Bragg diffraction peak reflectivity, peak position and corresponding bilayer spacing value, and peak FWHM is shown in Table 1.

The X-ray photoemission spectroscopy (XPS) measurements presented in the next section were performed using a Physical Electronics PHI model 5400 instrument. The spectra were obtained using Mg Kα radiation with a source power of 400 W. The analyzer pass energy was set at 35.75 eV for the high resolution measurements and the spectra were calibrated by setting the C (1s) line to 284.6 eV. A linear least-squares fitting procedure, employing a linear combination of Gaussian and Lorentzian peak shapes, was used to analyze the data.

3. Measurements and analysis

3.1. Ti–Be multilayers

Reflectivities were measured from all ten samples; eight multilayers and two bulk depositions of titanium and beryllium. In order to be an effective component of a supermirror, the reflectivity at the first order Bragg peak should be very close to unity. The highest first order Bragg peak reflectivity observed in this work was that of sample M92, a 40 bilayer deposition with a bilayer spacing of 108 Å (see Table 1). This measurement is shown in Fig. 1, together with the data from the other 110 Å bilayer thickness depositions.

Comparing the neutron reflectivity profiles in Fig. 1, the magnitude of the first order peak increases as n, the number of bilayers, increases from 10 to 20, as expected [11]. However, when n is increased to 30 and 40, the peak reflectivity does not continue to increase. It appears to saturate at a total reflectivity of approximately 60–65%. Fig. 2 shows the data from three of the four 90 Å depositions. These data also show a very pronounced shoulder on the low-Q side of the Bragg peak. The low saturation point and the first-order-peak shoulder are clear indications that disorder in the bilayer spacing exists. We also observed a second order diffraction peak in all of the multilayers measurements, as illustrated in Fig. 1. (The

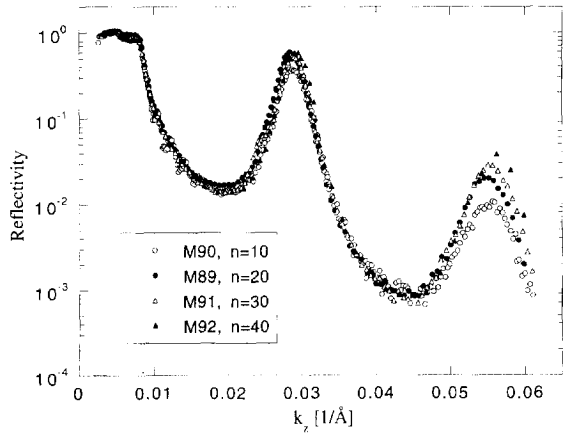

Fig. 1. Neutron reflectivity measurements of the larger bilayer spacing Ti–Be multilayers, M90, M89, M91 and M92.

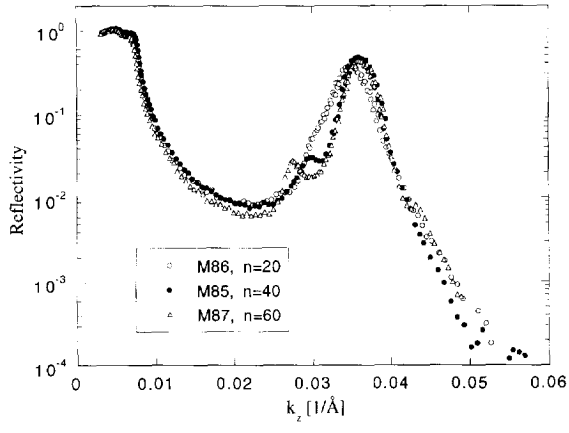

Fig. 2. Neutron reflectivity measurements of smaller bilayer spacing Ti–Be multilayers, M86, M85 and M87. The presence of a shoulder peak on the low-Q side of the first order peak is an indication of significant bilayer-spacing disorder in the depositions.

data from the 90 Å deposition set in Fig. 2 are truncated before complete resolution of the second order peak because of poor counting statistics.) All even order diffraction peaks are eliminated, theoretically, when the two components of the bilayer have equal thickness ($\Gamma = 0.5$) [11]. The presence of the second order peaks signifies unequal bilayer components, as is further demonstrated by a fit to the M90 data described next.

A fit of the M90 reflectivity data was performed using a genetic algorithm code developed at Argonne National Laboratory by De Haan and Drijkoningen [12]. (Due to the number of variable parameters, a fit to the large-n

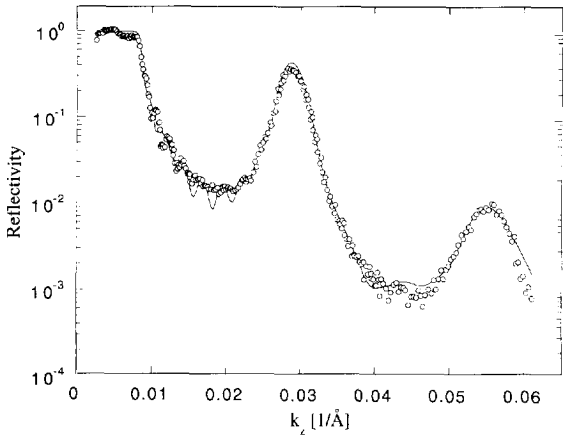

Fig. 3. Experimental data (open circles) and best fit (solid line) of the ten bilayer spacing M90 multilayer deposition. The main features of the measurement, the first and second order peaks, are reproduced by the fit.

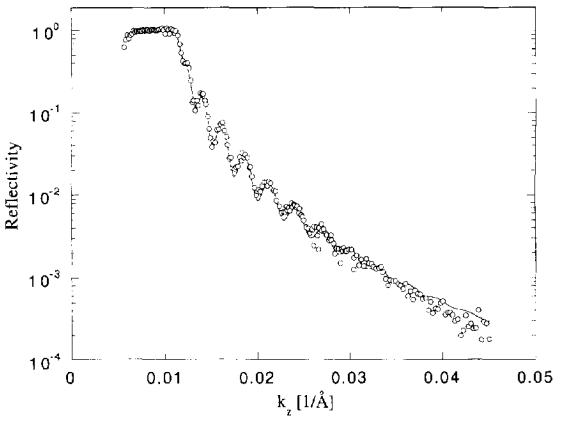

Fig. 4. Neutron reflectivity data (open circles) and best fit (solid line) of the bulk Be deposition, M93 (see text).

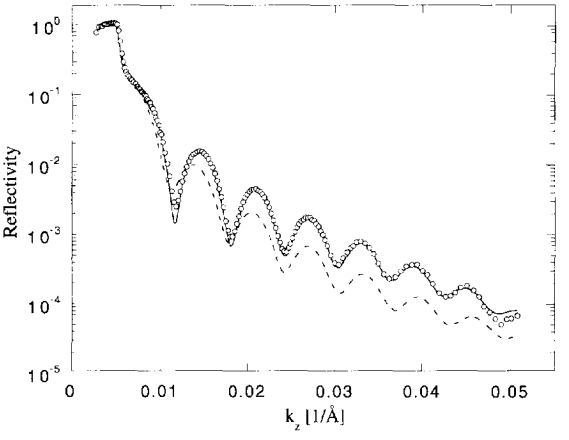

Fig. 5. Neutron reflectivity data (open circles) and best fit (solid line) of the bulk Ti deposition, M94. The dashed line represents a best fit to the experimental data without the inclusion of a surface oxide layer. The solid line fit was performed by sub-dividing the surface oxide into 10 layers (see text and Fig. 6).

multilayer depositions is nearly impossible with this algorithm.) The full range of merged measurements of M90 and the calculated reflectivities for the fitted profile are shown in Fig. 3. The scattering length densities for Ti and Be used to fit the M90 data were obtained from fits of the bulk depositions presented below. The fit to the M90 data is consistent with an average Be and Ti layer spacing of 72 and 42 Å ($\Gamma = 0.63$), respectively. The fit is not perfect, nor unique, but it reproduces the important features of the measurement. The fitting result also suggests considerable thickness disorder near the bottom of the multilayer deposition. We believe that this disorder results in a broadening of the first order peak and an increase in the magnitude of the valley between the critical edge and the first order peak.

3.2. *Bulk Ti and Be depositions*

The scattering length densities (Nb) for the as-deposited Be and Ti were obtained by fitting the data from the two bulk depositions, M93 and M94. This data and corresponding best-fits are shown in Figs. 4 and 5. The fitted values for Be and Ti are 10.3×10^{-6} and -2.2×10^{-6} Å^{-2}, respectively. These are in good agreement with the theoretical values for crystalline Be and Ti of 9.6×10^{-6} Å^{-2} and -1.95×10^{-6} Å. This is not proof, however, that the bulk Be deposition is indeed crystalline. The Be value is also in close agreement with the theoretical value of Be oxide (BeO), 9.96×10^{-6} Å^{-2}. The incorporation of large quantities of oxygen into the Be or Ti depositions was not expected in the UHV deposition chamber. At least for the bulk Be deposition, however, the neutron reflectivity measurement cannot distinguish between the pure component and oxide.

The situation is quite different for Ti oxide; the dashed line in Fig. 5 is a best fit to the experimental data without an oxide cap layer. This is a clear demonstration of the sensitivity of the neutron reflectometry technique to the presence of the Ti surface oxide. The Nb profile obtained from the best fit of the bulk Ti deposition, M94, including the oxide cap layer, is given in Fig. 6. Our motivation for sub-dividing the Ti surface oxide into ten separate layers, as indicated in Fig. 6, requires explanation. In our first attempt at fitting the Ti bulk deposition data, we included a single, undivided oxide layer, using Nb and the

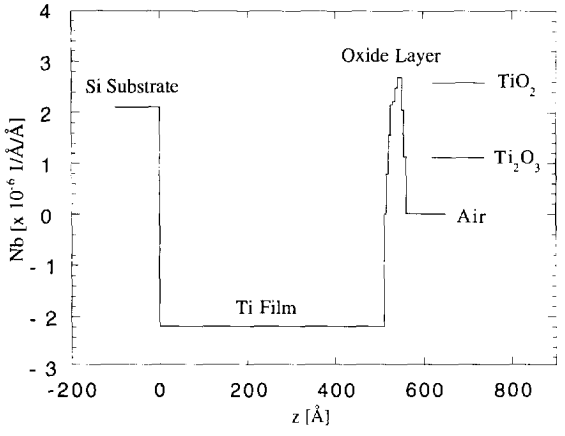

Fig. 6. Scattering length density profile of the bulk Ti deposition obtained from the best fit of M94. The surface oxide profile, which was sub-divided into ten layers in the best fit, is consistent with XPS measurements of the M94 deposition (see text and Fig. 7). The TiO_2 and Ti_2O_3 oxide Nb values are identified on the right-hand side of the figure.

thickness as fitting variables. The resulting fit (not shown) was very good, resulting in $Nb = 2.1 \times 10^{-6}$ Å^{-2} and a thickness of 48 Å. This Nb value does not, however, correspond to either of the two common native Ti oxides [13], TiO_2 (2.6×10^{-6} Å^{-2}, rutile structure) and Ti_2O_3 (1.1×10^{-6} Å^{-2}, hexagonal structure of the corundum type).

3.2.1. XPS of the Ti surface oxide

The Ti surface oxide of sample M94 was further characterized with X-ray photoemission spectroscopy (XPS) and this measurement is shown in Fig. 7. The two TiO_2 peaks are the most obvious at all angles (θ defined such that 90° is normal to the surface), indicating that the surface oxide layer is comprised primarily of this structure. What is not obvious at first is the presence of the $Ti_2O_3(\frac{3}{2})$ peak on the shoulder of the $TiO_2(\frac{3}{2})$ peak. The XPS curve fitting routine resolved this peak, along with the TiO_2 and Ti peaks, at all angles. This data is presented in Table 2 in the form of peak area as a function of angle.

The XPS measurements at 90° imply that approximately 13% of the oxide layer consists of Ti_2O_3. The XPS peak areas in Table 2 were used in a quantitative manner to calculate a smeared, or averaged, oxide layer scattering length density. These calculated values, shown in the last column of Table 2, simply used the XPS peak area fraction at each angle as a weighting factor. In other words, the fraction of TiO_2 and Ti_2O_3, assumed to be equal to the corresponding peak area fraction in Table 2, was used to calculate the total Ti and O atomic density in

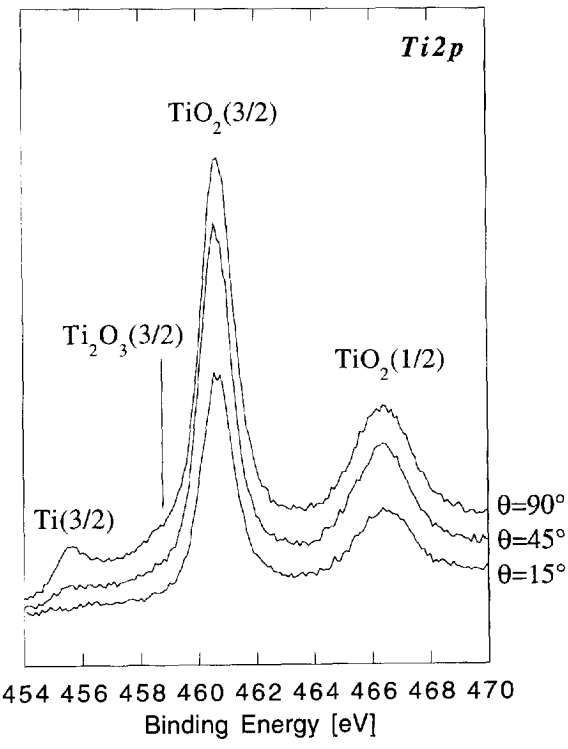

Fig. 7. XPS data at three takeoff angles (defined such that the 90° is the surface normal) of the bulk Ti M94 surface oxide. The two TiO_2 peaks are the most prominent in the spectra. However, the Ti_2O_3 peak on the low binding energy side of the $TiO_2(\frac{3}{2})$ peak was resolved by the XPS fitting procedure (see text).

Table 2
XPS results from Ti bulk deposition and calculated neutron scattering length densities

Angle, θ	Peak	Peak Area fraction	Nb [$\times 10^{-6}$ Å^{-2}]
15°	—	—	2.3
	$TiO_2(\frac{3}{2})$	87.8	
	$Ti_2O_3(\frac{3}{2})$	7.6	
	$Ti(\frac{3}{2})$	4.6	
45°	—	—	2.2
	$TiO_2(\frac{3}{2})$	82.7	
	$Ti_2O_3(\frac{3}{2})$	11.3	
	$Ti(\frac{3}{2})$	6.0	
90°	—	—	2.0
	$TiO_2(\frac{3}{2})$	78.2	
	$Ti_2O_3(\frac{3}{2})$	11.5	
	$Ti(\frac{3}{2})$	10.3	

the oxide layer, N_{Ti} and N_O, based on the known crystal structures. The averaged scattering length density of the oxide layer found in Table 2 is then given by $(Nb)_{oxide} = N_{Ti}b_{Ti} + N_O b_O$.

The averaged, or smeared, Nb values derived from the 45° and 90° XPS data both agree well with the neutron reflectivity Nb fitting result for the undivided oxide layer, 2.1×10^{-6} Å^{-2}. Thus, the neutron reflectivity measurement is consistent with the XPS result of an oxide layer consisting of approximately 13% Ti_2O_3 and the balance TiO_2. The fit to bulk Ti deposition presented in Fig. 6, with the surface oxide sub-divided into 10 layers, was performed in an effort to derive a finer scattering length density profile. Notice in Fig. 6 that the oxide portion of the profile rises rapidly from the air interface to the TiO_2 value. This is evidence, we believe, that the TiO_2 majority resides in the upper most portion of the surface oxide.

This hypothesis is supported by the XPS data in Table 2; the relative strength of the $TiO_2(\frac{3}{2})$ peak increases as θ decreases and the measurement probes volumes closer to the surface. Furthermore, the corresponding *decrease* in relative peak strength of the $Ti_2O_3(\frac{3}{2})$ peak in Table 2 at shallower takeoff angles is also consistent with the Ti_2O_3 oxide component residing near the metal–oxide interface. This last statement is supported to a certain degree by the Nb profile in Fig. 6; the more gradual fall-off from the maximum oxide Nb value to the bulk Ti value may be consistent with an intermediate Ti_2O_3 suboxide step at the Ti–oxide interface.

A similar conclusion has been drawn by Jobin et al. from XPS measurements of oxidized Ti surfaces [14]. In fact these authors obtained XPS spectra nearly identical to those presented here in Fig. 7. Based on the slight increases in $Ti_2O_3(\frac{3}{2})$ peak definition as the takeoff angle approached the surface normal, Jobin et al. concluded that Ti_2O_3 existed as a suboxide at the metal–oxide interface [14].

4. Conclusions

1. Eight magnetron sputtered, single-bilayer-spacing Ti–Be multilayer depositions have been characterized with neutron reflectometry. The measured superlattice peak reflectivities varied between approximately 40–60%. In the best case, deposition M92, a 64% peak reflectivity was observed. Well defined shoulder subpeaks were evident in some of the measurements, implying significant bilayer-spacing disorder. We believe such disorder exists in all the depositions and is responsible, at least in part, for the low reflectivities.

2. A fit to a ten-bilayer deposition reproduced the important features of the measurement, including a well resolved second-order peak. The presence of a second order peak signifies that $\Gamma \neq 0.5$, and the fit gave a value of $\Gamma = 0.63$.

3. Bulk Ti and Be depositions were characterized with neutron reflectivity as well. As-deposited Ti and Be scattering length densities derived from the data fitting procedure were in good agreement with theoretical values, although the absolute value of the Ti density was approximately 10% larger than the theoretical value.

4. A 48 Å oxide cap layer was required to properly fit the bulk Ti measurement. However, the scattering length density of the oxide layer determined from the first fitting attempt did not agree with values for the two common native Ti oxide structures, Ti_2O_3 and TiO_2. XPS measurements of the surface oxide indicated a mixture of approximately 13% Ti_2O_3 and 87% TiO_2. The scatering length density for the oxide layer calculated using these fractions was then in very good agreement with the neutron reflectivity value.

5. The XPS data indicate a segregation of the two oxide types, with the Ti_2O_3 residing at or near the metal–oxide interface and the thicker TiO_2 layer at the air–oxide interface. This segregation was supported by a second fit to the neutron reflectivity data with the surface oxide sub-divided into ten layers. The scattering length density profile from this fit rose rapidly from the air–oxide interface to the TiO_2 value, and then decreased more gradually to the Ti bulk level. The more gradual decrease may be consistent with an intermediate Ti_2O_3 step near the metal–oxide interface.

Acknowledgements

The authors are very grateful to C. Alford, Department of Chemistry and Material Science, LLNL, for performing the depositions. The ANL work is supported by the US DOE, BES-Materials Sciences, under contract No. W-31-109-ENG-38. The XPS measurements were carried out at the Center for Microanalysis of Materials, University of Illinois, which is supported by the US DOE under grant DEFG02-91-ER45439. In addition, the help of R. Haasch at the University of Illinois with the XPS measurements is gratefully acknowledged.

References

[1] J.B. Hayter and H.A. Mook, J. Appl. Crystallogr. 22 (1989) 35.

[2] See for example C.F. Majkrzak and J.L. Wood (eds.), Neutron Optical Devices and Applications, Proc. SPIE 1738 (1992).

[3] J.E. Keem, J. Wood, N. Grupido, K. Hart, S. Nutt, D.G. Reichel and W.B. Yelon, in: Thin-Film Neutron Optical Devices, ed. C.F. Majkrzak, Proc. SPIE 983 (1989) 38.
[4] J.L. Wood, in Neutron Optical Devices and Applications, eds. C.F. Majkrzak and J.L. Wood, Proc. SPIE 1738 (1992) 22.
[5] Z. Jiang, B. Vidal, M. Brunel, M. Maaza and F. Samuel, in: Neutron Optical Devices and Applications, eds. C.F. Majkrzak and J.L. Wood, Proc. SPIE 1738 (1992) 141.
[6] O. Elsenhans, P. Böni, H.P. Friedli, H. Grimmer, P. Buffat, K. Leifer and I. Anderson, in: Neutron Optical Devices and Applications, eds. C.F. Majkrzak and J.L. Wood, Proc. SPIE 1738 (1992) 130.
[7] C.F. Majkrzak and J.F. Ankner, in: Neutron Optical Devices and Applications, eds. C.F. Majkrzak and J.L. Wood, Proc. SPIE 1738 (1992) 150.
[8] B. Ballot, F. Samuel and B. Farnoux, Physica B 198 (1994) 220.
[9] Beryllium powder and dust are highly toxic when inhaled and proper precautions must be used during deposition.
[10] A. Karim, B.H. Arendt, R. Goyette, Y.Y. Huang, R. Kleb and G.P. Felcher, Physica B 173 (1991) 17.
[11] V.F. Sears, Acta Crystallogr. A 39 (1983) 601.
[12] V.O. DeHaan and G.G. Drijkoningen, Physica B 198 (1994) 24.
[13] A.D. McQuillan and M.K. McQuillan, Titanium (Academic Press, New York, 1956) p. 252.
[14] M. Jobin, M. Taborelli and P. Descouts, J. Appl. Phys. 77 (1995) 5149.